Directly probing spin dynamics in insulating antiferromagnets using ultrashort terahertz pulses

P. Bowlan, S. A. Trugman, X. Wang, Y. M. Dai, S.-W. Cheong, E. D. Bauer, A. J. Taylor, D. A. Yarotski, and R. P. Prasankumar

Phys. Rev. B **94**, 184429 — Published 22 November 2016

DOI: 10.1103/PhysRevB.94.184429

Directly probing spin dynamics in insulating antiferromagnets using ultrashort terahertz pulses

P. Bowlan,[1,*] S. A. Trugman,[1] X. Wang,[2] Y. M. Dai,[1] S.-W. Cheong,[2]
E. D. Bauer,[3] A. J. Taylor,[1] D. A. Yarotski,[1] and R. P. Prasankumar[1,†]

[1]*Center for Integrated Nanotechnologies, MS K771, Los Alamos National Laboratory, Los Alamos, New Mexico 87545, USA*
[2]*Rutgers Center for Emergent Materials and Department of Physics and Astronomy, Rutgers University, 136 Frelinghuysen Road, Piscataway, New Jersey 08854, USA*
[3]*Condensed Matter and Magnet Science Group, MS K764 Los Alamos National Laboratory, Los Alamos, New Mexico 87545, USA*

(Dated: October 24, 2016)

We investigate spin dynamics in the antiferromagnetic (AFM) multiferroic $TbMnO_3$ using optical-pump, terahertz (THz)-probe spectroscopy. Photoexcitation results in a broadband THz transmission change, with an onset time of 25 ps at 10 K that becomes faster at higher temperatures. We attribute this time constant to spin-lattice thermalization. The excellent agreement between our measurements and previous ultrafast resonant x-ray diffraction measurements on the same material confirms that our THz pulse directly probes spin order. Furthermore, the presence of a pump-probe signal above the magnetic ordering temperatures suggests that unlike resonant x-ray probing, THz transmission is sensitive to the dynamics of short range spin order, which is known to be of importance in spin-spiral multiferroics like $TbMnO_3$.

PACS numbers: 78.47.jh,75.50.Ee,75.85.+t

I. INTRODUCTION

The ability to switch the magnetization (M) in a ferromagnet (FM) on an ultrafast timescale is a longstanding area of fundamental interest, particularly due to its potential applications in magnetic data storage. However, ultrafast control of antiferromagnetic (AFM) materials using femtosecond laser pulses is arguably more promising, since their zero net magnetization makes it easier for the system to change while still conserving the total spin, so that in general their spin dynamics should be much faster than in FMs[1]. Multiferroic AFM manganites (e.g., $RMnO_3$, where R is a rare earth atom), which can have coexisting and coupled magnetic and ferroelectric orders, have attracted particular interest for their potential device applications[2]. Improved control and understanding of AFM order in multiferroics could influence practical applications such as four-state memory, ultrafast magnetoelectric switching[3], or magnetoelectric data storage[4].

Although AFM materials are potentially very useful, their magnetization, especially its temporal evolution, is more difficult to detect, making them less well understood. This is because optical methods for detecting spin order and its dynamics, such as the magneto-optical Kerr effect, are usually only sensitive to a non-zero magnetic moment, M[1]. Optical magnetic linear dichroism can instead be used to probe AFM order[5]; however, the presence of non-magnetic sources of birefringence can make this signal difficult to interpret. Optical second harmonic generation (SHG) is sensitive to AFM spin order and its dynamics[6–8], but when applied to multiferroics it must be distinguished from the larger SHG signal originating from ferroelectric order. The other option for probing ultrafast AFM spin dynamics is to use resonant x-ray diffraction with femtosecond x-ray pulses from large scale free electron lasers or synchrotrons[9–11], which are difficult to gain access to.

Considering that it is still not straightforward to measure ultrafast spin dynamics in AFMs, we recently introduced a simple, table-top method that probes AFM spin dynamics through a magnon resonance using terahertz (THz) pulses[12]. Applying this to the AFM multiferroic $HoMnO_3$, after photoexciting electrons with an optical pulse, we observed an induced transparency for the THz probe pulse only at the magnon resonance, clearly indicating a direct sensitivity to spin order. Further analysis of our data showed a change in the magnon line shape (its frequency, amplitude and linewidth) on a timescale of 5-12 picoseconds (ps) that vanished above the Neel temperature T_N, which was due to spin-lattice thermalization. Furthermore, for temperatures (T) less than T_N, the spin-lattice thermalization time τ becomes faster with increasing T in $HoMnO_3$, while the opposite happens in the FM manganites, such as $La_{0.7}Ca_{0.3}MnO_3$[13].

Here, we further illustrate that THz pulses are a rather general probe of ultrafast spin dynamics, applicable to a broader range of materials with different AFM spin alignments, by applying this technique to a system with a completely different type of spin order. We consider the orthorhombic multiferroic insulator $TbMnO_3$, which is antiferromagnetically ordered below $T_{N1} = 42$ K, where it is an incommensurate AFM, and also ferroelectric below $T_{N2} = 28$ K, where it becomes a commensurate AFM[14]. Very similar to that seen in $HoMnO_3$, the photoinduced change in THz transmission has a rise time of ∼18-25 ps, which we conclude also comes from spin-lattice thermalization. However, unlike $HoMnO_3$, where

the photoinduced changes occurred only at the magnon mode, they happen over the full THz pulse spectrum in $TbMnO_3$. Our data still links this to spin heating, confirmed by the excellent agreement of our results below T_{N1} with previous ultrafast resonant x-ray diffraction measurements[10]. However, in contrast to resonant x-ray diffraction, we find that THz probing is also sensitive to short range magnetic order, which was previously linked to a broad static absorption component in this frequency range[15]. Similarly, our photoinduced THz changes are spectrally broad and our pump-probe signal persists to slightly above T_{N1}. Our results thus further illustrate that THz pulses can provide a direct, tabletop probe of antiferromagnetic order, which can even be sensitive to short-range magnetic order.

II. RESULTS

The $TbMnO_3$ single crystals used in our experiments were grown in an optical floating zone furnace[14]. The crystal used in our measurements had the a and c axes in-plane and a thickness of $\sim$150 μm. Our optical-pump, THz-probe (OPTP) system was based on a 1 kHz Ti:sapphire amplifier producing pulses centered at 800 nm, with a duration of $\sim$40 femtoseconds (fs). Ultrashort THz pulses were generated by optical rectification in GaSe and measured by electro-optic sampling in ZnTe (similar to the setup in[16]). The THz probe and optical pump pulses were both linearly polarized along the a-axis and collinear. The absorption length for the optical pulse is only $\sim$200 nm [17], while the THz absorption length is closer to the entire crystal thickness, depending on the frequency and temperature (Fig. 1); the optical absorption thus determines the effective crystal length for our OPTP measurements. As discussed in our previous work on $HoMnO_3$, lateral diffusion (either heat or transport) is too slow to have any significant effect on our time constants (which might result from the pump and probe penetration depth mismatch)[12]. The fact that our THz transmission probe gives a very similar time constant to that measured with x-rays in reflection (discussed in more detail below), where the probe penetration depth is less than that of the pump, confirms this.

Fig. 1(a) shows the THz (T_R) transmission spectrum through our $TbMnO_3$ crystal as a function of temperature (T) without optical photoexcitation. No Drude-like response is seen (for comparison see the dashed black line), and instead the THz absorption is dominated by magnetic effects. Below T_{N2}, the two well-known electric-dipole active magnon modes, or electromagnons, in $TbMnO_3$ at $\sim$0.75 and 2 THz are apparent[18–20]. On top of these peaks, there is a continuum-like absorption feature with a full width of about 130 cm^{-1} (4 THz) which has been attributed to a band of infrared-active, two-magnon excitations[15,21,22]. This broad absorption is seen even above T_{N1}, since short range magnetic order has been observed to develop in $TbMnO_3$ well above the magnetic ordering temperatures[15,23]. In Fig. 1, the two-magnon absorption band is most apparent for $T > T_{N1}$, manifested as a broad, flat feature which slowly vanishes with increasing temperature (i.e., T_R increases), consistent with[15]. The oscillations in the transmission, which become visible at $\sim$30 K where there is less absorption, originate from the interference between reflections from the front and back surfaces of our $\sim$150 μm thick crystal.

Fig. 2(a) shows the time-dependent electric (E) field of the pulse transmitted through the crystal ($E_{trans}(t)$) at 10 K, which exhibits oscillations at later times (as compared to the E-field of the incident single cycle THz pulse in the inset of Fig. 2(a), $E_{in}(t)$) due to the electromagnon resonances. Next, we optically excited the $TbMnO_3$ crystal at 800 nm with a fluence of F=6 mJ/cm^2 (corresponding to $\sim 10^{22}$ carriers/cm^3 at 10 K, or $\sim$0.1 carrier/unit cell). The blue curve in Fig. 2(a) shows the resulting photoinduced change in the transmitted THz E-field ($\Delta E(t)/E_0$, defined in the caption of Fig. 2) for a pump-probe delay of τ=100 ps. At early gate delays (t = 0) the photoinduced THz transmission change is in phase with the transmitted THz pulse, representing a spectrally broad increase in transmission. The out-of-phase photoinduced changes at later times, where the oscillations from the electromagnons dominate, indicate that photoexcitation reduces the amplitude of these oscillations, or that the electromagnon absorption is decreasing. The spectra of the curves in Fig. 2(a) were computed with a Fourier transform and are shown in Fig. 2(b), along with the simulated changes in the transmitted THz spectrum due to the approximate heating introduced by the pump pulse. This allows us to make two important observations. First, in contrast with our measurements on $HoMnO_3$, the photoinduced changes happen across the entire THz pulse spectrum, not just at the electromagnon resonances. Second, as confirmed by the simulation, the photoinduced changes are consistent with the changes in the transmitted THz spectrum induced by heating.

To investigate the photoinduced dynamics, we measured $\Delta E/E_0$ versus both gate and pump-probe delays at T=10 K, as shown in Fig. 3(a) (with the spectrum shown in Fig. 3(b)). These images show that for all gate delays, or all frequencies across the transmitted THz pulse, the photoinduced transparency has the same pump-probe delay dependence and builds up over $\sim$25 ps. No further changes were seen up to the longest measured time delays of $\sim$300 ps. Fig. 4(a) shows pump-probe signals for different sample temperatures versus delay τ, measured at a fixed gate delay where the difference was largest (t = 0 ps in Fig. 2(a)). The amplitude ($\Delta E/E_0$) of the signals at τ = 100 ps for different temperatures is shown in Fig. 4(b). The right y-axis (dashed line) of this figure shows the instantaneous pump-induced heating, calculated from the heat capacity[24] and the pump fluence. The shape of this curve is in good agreement with the amplitude of the pump-probe signal versus temperature, strongly suggesting that the phonon temperature determines the amount of spin heating. In addition, using a single exponential

fit, we extracted the temperature-dependent rise time of the curves in Fig. 4(a), shown in Fig. 4(c). We fit the temperature dependence of the resulting time constants to a power law, T^Q, finding $Q = -0.2$. The fluence dependence of the time constant τ_R and the amplitude of the OPTP signals are plotted in Fig. 5 for T=10 K, t=0 ps. Note that at a fluence of 6 mJ/cm^2 we estimate ∼4 K steady state heating, using the model from [25] and the thermal conductivity given in ref. [26], which is approximately constant over the 10-50 K temperature range that we consider. We have adjusted all of the temperature axes in Fig. 4 by this amount relative to our cryostat settings.

III. DISCUSSION

Several features of our data indicate that THz pulses can directly probe spin order in $TbMnO_3$. In our previous work on $HoMnO_3$[12] this was more obvious since the photoinduced changes occurred only at the magnon resonance, while in $TbMnO_3$, the spectral changes happen across the whole THz spectrum (Fig. 2(b)). Here, the most compelling evidence comes from a comparison of our measurements to a recent optical-pump, resonant x-ray diffraction study on $TbMnO_3$[10], since that method is already known to be a direct, ultrafast probe of spins[9]. Our THz data agrees very well with those measurements. In both cases a single exponential rise was observed (Fig. 4) with a time constant of ∼23 ps for T=11-12 K and F= 6 mJ/cm^2. The x-ray study indicated that this was associated with a melting of spin order (through heating the spin system). Our measured fluence dependence, shown in Fig. 5, also agrees well with the trends shown in the resonant x-ray diffraction study (see Fig. 3 in ref.[10]), since in both cases the amplitude of the OPTP signal saturates at ∼6 mJ/cm^2. We note that the time constant drops more rapidly with increasing fluence in the x-ray data[10]. Also in contrast to the x-ray data, the OPTP signal persists slightly above T_{N1}, while the resonant x-ray diffraction signal vanishes before this. As we discuss more below, we attribute both of these differences to the fact that THz probing is sensitive to short-range spin order (relevant at higher temperatures and fluences), a potential advantage of probing spin dynamics with THz pulses over other techniques.

Further evidence for the fact that we probe only spin dynamics, even though the photoinduced changes are broad and not just at the electromagnon resonances, comes from the continuum-like infrared active two-magnon excitation in the static THz absorption of $TbMnO_3$ discussed above[15]. This indicates that the observed static absorption features, including the electromagnons and the broad, flat background seen in Fig. 1, are all magnetic in origin, and hence their dynamics are too. This is also supported by the fact that the OPTP signal in $TbMnO_3$ persists above T_{N1} and slowly decreases above this temperature (it was no longer detectable above 54 K) [15,21]. Finally, if $TbMnO_3$ were not a good insulator, photoexcited electron-hole pairs would likely lead to a Drude response in the THz conductivity spectrum, which might dominate or obscure the spin dynamics. Fig 1 demonstrated the lack of any Drude response in the static THz spectrum, and Fig. 2(b) confirmed that the photoinduced spectral changes are also not consistent with a Drude response, but instead with heating. Therefore, we suggest that in general, THz pulses may be able to probe ultrafast spin dynamics in any insulating AFM system, as long as the static THz absorption is of magnetic origin.

Next, we argue that the time constant τ_R observed in our OPTP measurements is due to spin-lattice thermalization. Our 800 nm pump pulse photoexcites intersite Mn-Mn electron transitions in orthorhombic $TbMnO_3$. Given that we observe spin heating in our OPTP measurements, and that the energy from optical photoexcitation is deposited in the electrons, the next question is how electrons transfer energy to the spins. Our THz data in Figs. 3 and 4 does not show the initial fast transfer of energy from electrons to phonons that is normally observed in manganites, most likely because of our limited time resolution (∼250 fs). However, optical-pump/optical-probe measurements on $TbMnO_3$, which are directly sensitive to electronic order, show that this process occurs within ∼30-100 fs of photoexcitation [27,28]; this is typical for manganites (see, e.g., [29,30]). Therefore, before the ∼18-25 ps relaxation process described by τ_R occurs, the electrons and phonons have already thermalized, pointing towards a phonon-mediated transfer of energy from electrons to spins (also often seen in manganites[31]). Further evidence for this comes from the ultrafast lattice heating calculations in Fig. 4(b), showing that our estimate of the photoinduced lattice temperature increase agrees well with the measured spin temperature increase shown in Fig. 4(a) of ref.[10], both of which are ∼ 27 K. The above considerations thus indicate that after the relaxation process shown in Figs. 4(c) and 5(b), the spins and lattice are in thermal equilibrium, allowing us to ascribe τ_R to spin-lattice thermalization (as in ref. [12]). We suggest that the importance of short-range magnetic order in $TbMnO_3$[15,23], apparent also from the fact that our OPTP signal persists above T_{N1}, as well as the temperature dependence of the broad two-magnon excitation, could account for the slower spin-lattice relaxation in $TbMnO_3$ as compared to $HoMnO_3$[12], where such a feature was not present. This is also consistent with all-optical pump-probe measurements on $Eu_{0.75}Y_{0.35}MnO_3$, a system also known to have short range magnetic order above T_N[21], which showed a relaxation time similar to that seen here that also slowly decreases in amplitude above T_N[32].

We now discuss the microscopic mechanism by which spin-lattice thermalization could occur in $TbMnO_3$ and other AFM systems. Previous ultrafast studies on orthorhombic AFM $RMnO_3$ compounds[10,32] proposed that the formation of optically induced polarons could play

a role in ultrafast spin heating. As described above, in the orthorhombic manganites, absorption of light at 800 nm is associated with Mn-Mn inter-site transitions, changing the charge of the ions and resulting in the formation of small polarons[33]. In contrast, optical excitation of hexagonal manganites such as $HoMnO_3$ results in on-site transitions and a very small perturbation of the polaronic potential, yet a similar spin-lattice relaxation time was observed in this system[12]. Also, the formation and relaxation of optically excited polarons observed in other manganites and semiconductors typically takes place in < 1 ps[34–36] due to the small spatial scales involved. Considering these facts and that a range of different AFM systems all show similar monotonically decreasing spin-lattice thermalization times with temperature[12,27,28,32,37], we suggest that instead of involving excitations associated with a specific type of spin or lattice order (such as polarons), the microscopic mechanism governing spin-lattice relaxation in these compounds could instead more generally be related to the fact that they are all AFMs.

To learn more about this trend in AFMs, we consider the commonly used two-temperature model (TTM) for the spin-lattice thermalization time, τ_{SL}. Ref.[38] shows that this is given by C_s/g, where C_s is the spin specific heat and g is the spin-lattice coupling constant, under the assumption that C_s is much smaller than the lattice specific heat. In FMs, one can assume that g has no temperature dependence[39], since $\tau_{SL}(T)$ follows the temperature dependence of $C_s(T)$[13,40], and therefore, like C_s, peaks at the Curie temperature. Similarly, τ_R in $TbMnO_3$ (Fig. 4(c)), as well as some of the other AFM systems discussed above[27,32], also shows peaks at the Neél temperatures T_{N1} and T_{N2}, following the peaks in C_s[24]. However, a strong monotonic decrease in τ_R with temperature is also seen on top of this, as described by the power law fit shown in Fig. 4(c). This suggests that, unlike the FM manganites, the spin-lattice coupling constant g has a stronger, non-negligible temperature dependence in AFMs, pointing to a fundamental difference in the way that spins and phonons couple in these two types of systems.

As discussed in our previous paper[12], we can gain insight into differences in spin-lattice thermalization between FM and AFM systems by considering that the simplest Hamiltonian for spin-lattice thermalization involves an exchange constant $J(r)$, where r is the distance between atoms. Through this type of interaction, phonons exchange energy with spins by directly modulating $J(r)$. This Hamiltonian conserves the net magnetization M and can therefore heat spins in AFMs, where $M = 0$, even in the spin ordered state. However this Hamiltonian cannot account for spin heating in FMs, in which $M \neq 0$; spin-lattice relaxation in this case happens instead through interactions that reduce M, such as spin-orbit coupling[41]. Consistent with this argument, spin-orbit coupling is usually weak in $RMnO_3$ compounds because of crystal field quenching, making spin-lattice thermalization slower in the FM manganites (e.g.,[13,40]). Therefore, another possible, potentially larger microscopic mechanism for spin-lattice thermalization in AFMs (in addition to spin-orbit coupling) is direct heating of spins by phonons through the exchange interaction.

To test this idea, we follow the Boltzmann rate equation model of[42], based on a Hamiltonian for spin-lattice thermalization with direct coupling through the exchange interaction $J(r)$. Although this was originally intended for FMs, before it was shown that a more complex Hamiltonian was needed[41], we propose that it could apply to AFMs, where this term may dominate over spin-orbit coupling. Specifically, this interaction is computed by considering the leading magnon-phonon scattering process, which in this case, is one phonon creating one magnon and annihilating another. The calculation therefore depends on the magnon and phonon dispersions of the material, as well as the populations of these particles, which gives the resulting thermalization time a strong temperature dependence. Applying this model to $HoMnO_3$, we were able to reproduce a monotonically decreasing τ_{SL} for $T < T_N$, as in our measurements (both here and in [12]). However, the calculated exponential describing the temperature dependence was T^{-3}, which is faster than the measured $T^{-0.5}$ dependence in $HoMnO_3$; because of this discrepancy we have not yet attempted to apply this to $TbMnO_3$, but would expect a similar outcome. Some possible reasons for the discrepancy are that the model assumes that the spin and phonon subsystems thermalize instantaneously amongst themselves after scattering and that the magnetic anisotropy is temperature independent, which neutron studies on other manganites suggest may not be the case[43]. It may also be important to include spin-orbit coupling and consider the insulating nature of the AFM manganites, unlike most FMs. In the future, we plan to develop a more detailed quantitative model for spin-lattice relaxation in AFM manganites based on these ideas. We point out that until a better theoretical description is available, some of our conclusions about the differences in AFM and FM manganites are speculative. However, we think that these ideas are worth more consideration, considering that they could lead to new methods for optically controlling the exchange interaction in AFM materials by resonantly driving phonons.

IV. SUMMARY

We demonstrated that in the AFM multiferroic $TbMnO_3$, THz pulses can directly probe the dynamics of both long and short range spin order. In this material, we observed an optically induced transmission change that developed within 18-25 ps after photoexcitation. Excellent agreement with a previous ultrafast x-ray study confirms that we directly probe spin order, and that the observed dynamics originate from spin-lattice thermalization, as in our previous study of $HoMnO_3$[12]. The spec-

trally broad photoinduced THz transmission change persisting slightly above T_{N2}, consistent with a previously identified broad THz absorption feature due to short-range magnetic order, indicates that we also can probe the dynamics of short-range magnetic order in $TbMnO_3$, something which was not possible with resonant x-ray diffraction probing. This work thus demonstrates a powerful approach for directly probing AFM spin dynamics, which may be applicable to applicable to a wide range of insulating AFM systems. More generally, the idea of probing the ultrafast dynamics of order parameters through low energy resonances is applicable to phonons as well as magnons and can shed new light on the couplings between these resonances, which will be especially useful in unraveling the physics of correlated electron systems.

Acknowledgments

The ultrafast measurements were performed at the Center for Integrated Nanotechnologies, a U.S. Department of Energy, Office of Basic Energy Sciences user facility and also partially supported by the NNSA's Laboratory Directed Research and Development Program. Los Alamos National Laboratory, an affirmative action equal opportunity employer, is operated by Los Alamos National Security, LLC, for the National Nuclear Security Administration of the U. S. Department of Energy under contract DE-AC52-06NA25396. The work performed at Rutgers University was supported by the DOE under Grant No. DOE: DE-FG02-07ER46382. We thank Rolando Valdés Aguilar for helpful discussions.

* Electronic address: pambowlan@lanl.gov
† Electronic address: rpprasan@lanl.gov

[1] A. V. Kimel, A. Kirilyuk, A. Tsvetkov, R. V. Pisarev, and T. Rasing, Nature **429**, 850 (2004).
[2] M. M. Vopson, Critical Reviews in Solid State and Materials Sciences **40**, 223 (2015).
[3] Y. M. Sheu, S. A. Trugman, L. Yan, Q. X. Jia, A. J. Taylor, and R. P. Prasankumar, Nature Communications **5** (2014).
[4] J. Scott, Nature Materials **6**, 256 (2007).
[5] D. Bossini, A. M. Kalashnikova, R. V. Pisarev, T. Rasing, and A. V. Kimel, Physical Review B **89**, 060405 (2014).
[6] M. Fiebig, T. Lottermoser, D. Fröhlich, A. V. Goltsev, and R. V. Pisarev, Nature **419**, 818 (2002).
[7] N. P. Duong, T. Satoh, and M. Fiebig, Physical Review Letters **93**, 117402 (2004).
[8] Y. M. Sheu, N. Ogawa, Y. Kaneko, and Y. Tokura, Physical Review B **94**, 081107 (2016).
[9] R. Tobey, S. Wall, M. Först, H. Bromberger, V. Khanna, J. Turner, W. Schlotter, M. Trigo, O. Krupin, W. Lee, et al., Physical Review B **86**, 064425 (2012).
[10] J. A. Johnson, T. Kubacka, M. C. Hoffmann, C. Vicario, S. de Jong, P. Beaud, S. Grübel, S.-W. Huang, L. Huber, Y. W. Windsor, et al., Physical Review B **92**, 184429 (2015).
[11] T. Kubacka, J. A. Johnson, M. A. Hoffmann, C. Vicario, S. de Jong, P. Beaud, S. Grübel, S.-W. Huang, L. Huber, L. Patthey, et al., Science **343**, 1333 (2014).
[12] P. Bowlan, S. Trugman, J. Bowlan, J.-X. Zhu, N. Hur, A. Taylor, D. Yarotski, and R. Prasankumar, Physical Review B **94**, 100404 (2016).
[13] R. D. Averitt, A. I. Lobad, C. Kwon, S. A. Trugman, V. K. Thorsmølle, and A. J. Taylor, Physical Review Letters **87**, 017401 (2001).
[14] M. Kenzelmann, A. B. Harris, S. Jonas, C. Broholm, J. Schefer, S. B. Kim, C. L. Zhang, S. W. Cheong, O. P. Vajk, and J. W. Lynn, Physical Review Letters **95**, 087206 (2005).
[15] Y. Takahashi, N. Kida, Y. Yamasaki, J. Fujioka, T. Arima, R. Shimano, S. Miyahara, M. Mochizuki, N. Furukawa, and Y. Tokura, Physical Review Letters **101**, 187201 (2008).
[16] P. Bowlan, W. Kuehn, K. Reimann, M. Woerner, T. Elsaesser, R. Hey, and C. Flytzanis, Physical Review B **85**, 165206 (2012).
[17] M. Bastjan, S. G. Singer, G. Neuber, S. Eller, N. Aliouane, D. N. Argyriou, S. L. Cooper, and M. Rübhausen, Physical Review B **77**, 193105 (2008).
[18] A. Pimenov, A. A. Mukhin, V. Y. Ivanov, V. Travkin, A. M. Balbashov, and A. Loidl, Nature Physics **2**, 97 (2006).
[19] R. Valdés Aguilar, M. Mostovoy, A. B. Sushkov, C. L. Zhang, Y. J. Choi, S. W. Cheong, and H. D. Drew, Physical Review Letters **102**, 047203 (2009).
[20] R. V. Aguilar, *Electromagnons in multiferroic materials* (ProQuest, 2008).
[21] R. Valdés Aguilar, A. B. Sushkov, C. L. Zhang, Y. J. Choi, S.-W. Cheong, and H. D. Drew, Physical Review B **76**, 060404 (2007).
[22] N. Kida, Y. Takahashi, J. Lee, R. Shimano, Y. Yamasaki, Y. Kaneko, S. Miyahara, N. Furukawa, T. Arima, and Y. Tokura, JOSA B **26**, A35 (2009).
[23] R. Kajimoto, H. Yoshizawa, H. Shintani, T. Kimura, and Y. Tokura, Physical Review B **70**, 012401 (2004).
[24] N. P. Kumar, G. Lalitha, and P. V. Reddy, Physica Scripta **83**, 045701 (2011).
[25] J. Demsar, J. L. Sarrao, and A. J. Taylor, Journal of Physics: Condensed Matter **18**, R281 (2006).
[26] K. Berggold, J. Baier, D. Meier, J. A. Mydosh, T. Lorenz, J. Hemberger, A. Balbashov, N. Aliouane, and D. N. Argyriou, Physical Review B **76**, 094418 (2007).
[27] J. Qi, L. Yan, H. D. Zhou, J.-X. Zhu, S. A. Trugman, A. J. Taylor, Q. X. Jia, and R. P. Prasankumar, Applied Physics Letters **101**, 2904 (2012).
[28] I. Handayani, R. Tobey, J. Janusonis, D. Mazurenko, N. Mufti, A. Nugroho, M. Tjia, T. Palstra, and P. van Loosdrecht, Journal of Physics: Condensed Matter **25**, 116007 (2013).
[29] Y. T. Wang, C. W. Luo, and T. Kobayashi, Advances in Condensed Matter Physics **2013** (2013).
[30] S. Wall, D. Prabhakaran, A. T. Boothroyd, and A. Cavalleri, Physical Review Letters **103**, 097402 (2009).
[31] R. D. Averitt and A. J. Taylor, Journal of Physics: Condensed Matter **14**, R1357 (2002).
[32] D. Talbayev, J. Lee, S. A. Trugman, C. L. Zhang, S.-W. Cheong, R. D. Averitt, A. J. Taylor, and R. P. Prasanku-

mar, Physical Review B **91**, 064420 (2015).
[33] P. B. Allen and V. Perebeinos, Physical Review B **60**, 10747 (1999).
[34] R. P. Prasankumar, S. Zvyagin, K. V. Kamenev, G. Balakrishnan, D. M. Paul, A. J. Taylor, and R. D. Averitt, Physical Review B **76**, 020402 (2007).
[35] P. Gaal, W. Kuehn, K. Reimann, M. Woerner, T. Elsaesser, and R. Hey, Nature **450**, 1210 (2007).
[36] K. Wu, T. Hsu, H. Shih, Y. Chen, C. Luo, T. Uen, J.-Y. Lin, J. Juang, and T. Kobayashi, Journal of Applied Physics **105**, 043901 (2009).
[37] E. E. M. Chia, J.-X. Zhu, H. J. Lee, N. Hur, N. O. Moreno, E. D. Bauer, T. Durakiewicz, R. D. Averitt, J. L. Sarrao, and A. J. Taylor, Physical Review B **74**, 140409 (2006).
[38] R. H. M. Groeneveld, R. Sprik, and A. Lagendijk, Physical Review B **51**, 11433 (1995).
[39] E. Beaurepaire, J.-C. Merle, A. Daunois, and J.-Y. Bigot, Physical Review Letters **76**, 4250 (1996).
[40] A. I. Lobad, R. D. Averitt, C. Kwon, and A. J. Taylor, Applied Physics Letters **77**, 4025 (2000).
[41] Y. Yafet, in *Solid State Physics*, edited by T. D. Seitz, F. (Academic Press, New York, 1963), vol. 14, pp. 1–98.
[42] E. Abrahams and C. Kittel, Physical Review **88**, 1200 (1952).
[43] O. P. Vajk, M. Kenzelmann, J. W. Lynn, S. B. Kim, and S.-W. Cheong, Physical Review Letters **94**, 087601 (2005).

Figures

FIG. 1: (Color online) THz transmission, T_R, versus frequency ν (without optical photoexcitation) and sample temperature through a 150 μm thick *ac*-oriented $TbMnO_3$ crystal, with the THz E-field polarized along the crystal a-axis. T_R is defined as $|E_{trans}(\nu)/E_{in}(\nu)|$, where $E_{in}(\nu)$ is the incident THz pulse and $E_{trans}(\nu)$ is the transmitted pulse. The dashed, grey lines indicate the positions of the electromagnon resonances. The dashed black line shows a calculated Drude response.

FIG. 2: (Color online) (a) THz E-field versus time transmitted through the crystal (red) ($E_{trans}(t)$) without photoexcitation, and the photoinduced change versus time in the THz E-field (blue) given by $\Delta E/E_0 = (E_{pumped}(t) - E_{trans}(t))/E_0$ and normalized to the maximum of E_{trans}, E_0. These curves were measured at τ=100 ps. The inset shows the THz E-field before the $TbMnO_3$ crystal, $E_{in}(t)$. (b) The spectra of the curves in Fig. 2(a). The purple, dashed line simulates how the transmitted THz spectrum changes with 24 K of heating, calculated by Fourier transforming ($E_{trans}(t)$(30 K)-$E_{trans}(t)$(6 K)) and taking the absolute value of the result. All other curves were measured at $T \sim$6 K.

FIG. 3: (Color online) (a) Photoinduced change in the transmitted THz pulse, $\Delta E/E_0$, versus gate delay t and pump-probe delay τ at T=10 K. (b) The Fourier transform of (a), showing $|\Delta E(\nu,\tau)/E_0|$, i.e., the power spectrum versus τ. The grey dashed lines at 0.75 and 2 THz show the positions of the electromagnons.

FIG. 4: (Color online) (a) OPTP signals at different temperatures for t=0 ps and F = 6 mJ/cm^2. (b) Amplitude of the OPTP signals versus temperature. The right y-axis shows the pump-induced heating (dashed line), calculated from the heat capacity and fluence[24]. (c) The rise time of the OPTP signals versus T, extracted from an exponential fit. The blue dashed line is a power law fit, where the power Q= -0.2. In both (b) and (c), the dashed lines show the transition temperatures T_{N1} and T_{N2}.

FIG. 5: (Color online) (a) The amplitude and (b) time constant τ_R extracted from OPTP signals measured at 10 K for different fluences and t=0 ps. The dashed, grey line in (a) illustrates the linear dependence of the amplitude on fluence up to 7 mJ/cm^2.

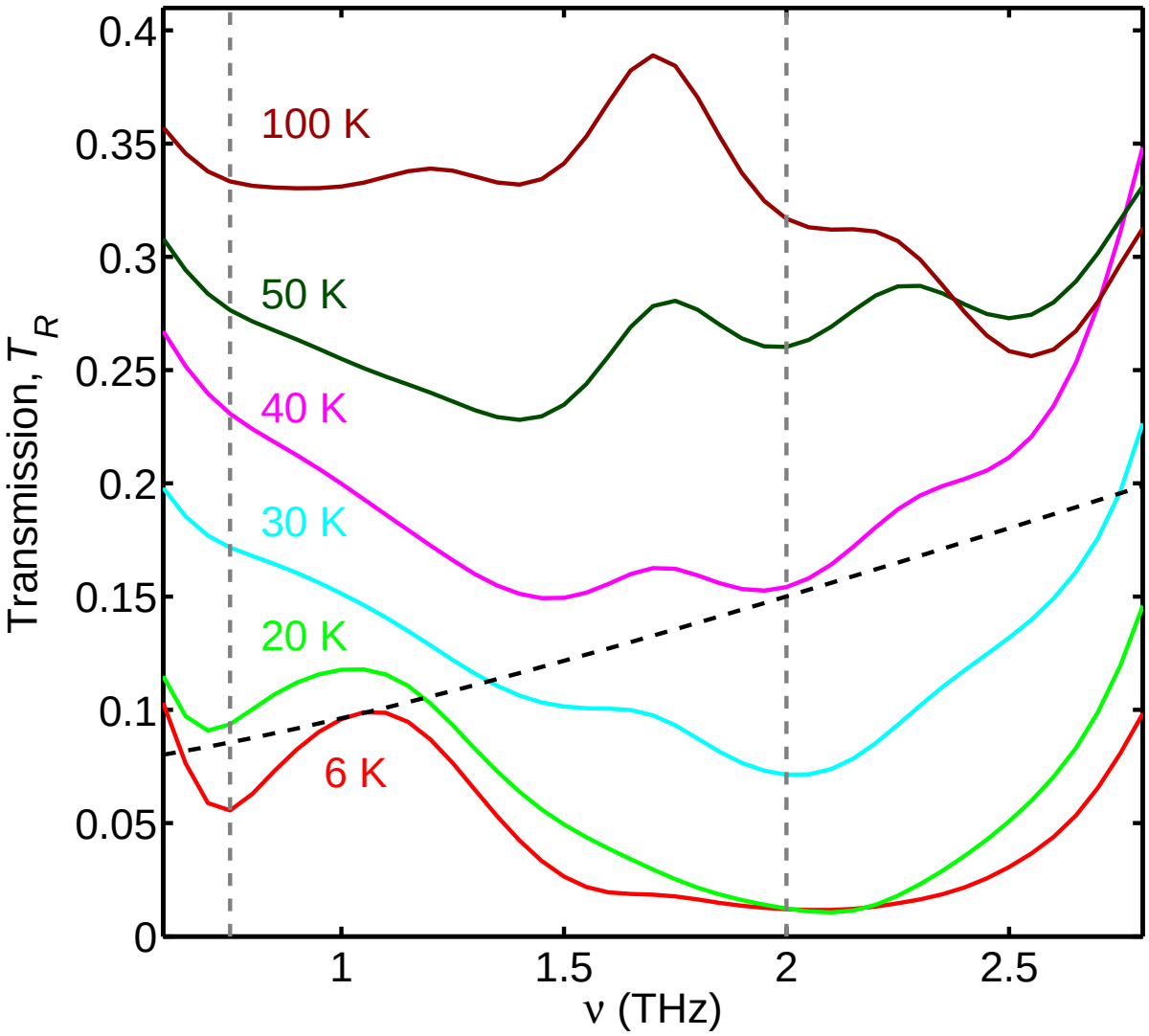

Figure 1 24Oct2016

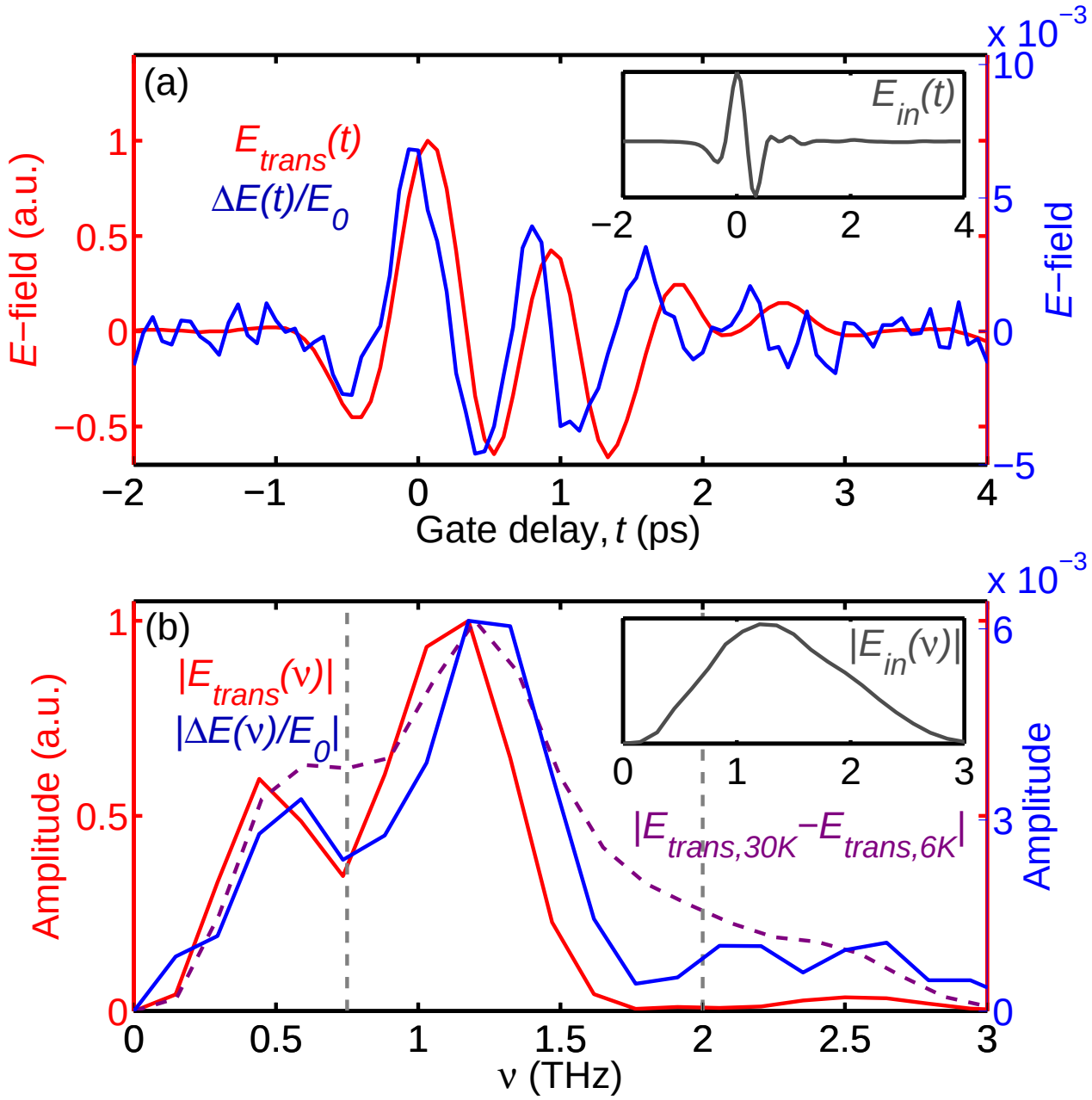

Figure 2 24Oct2016

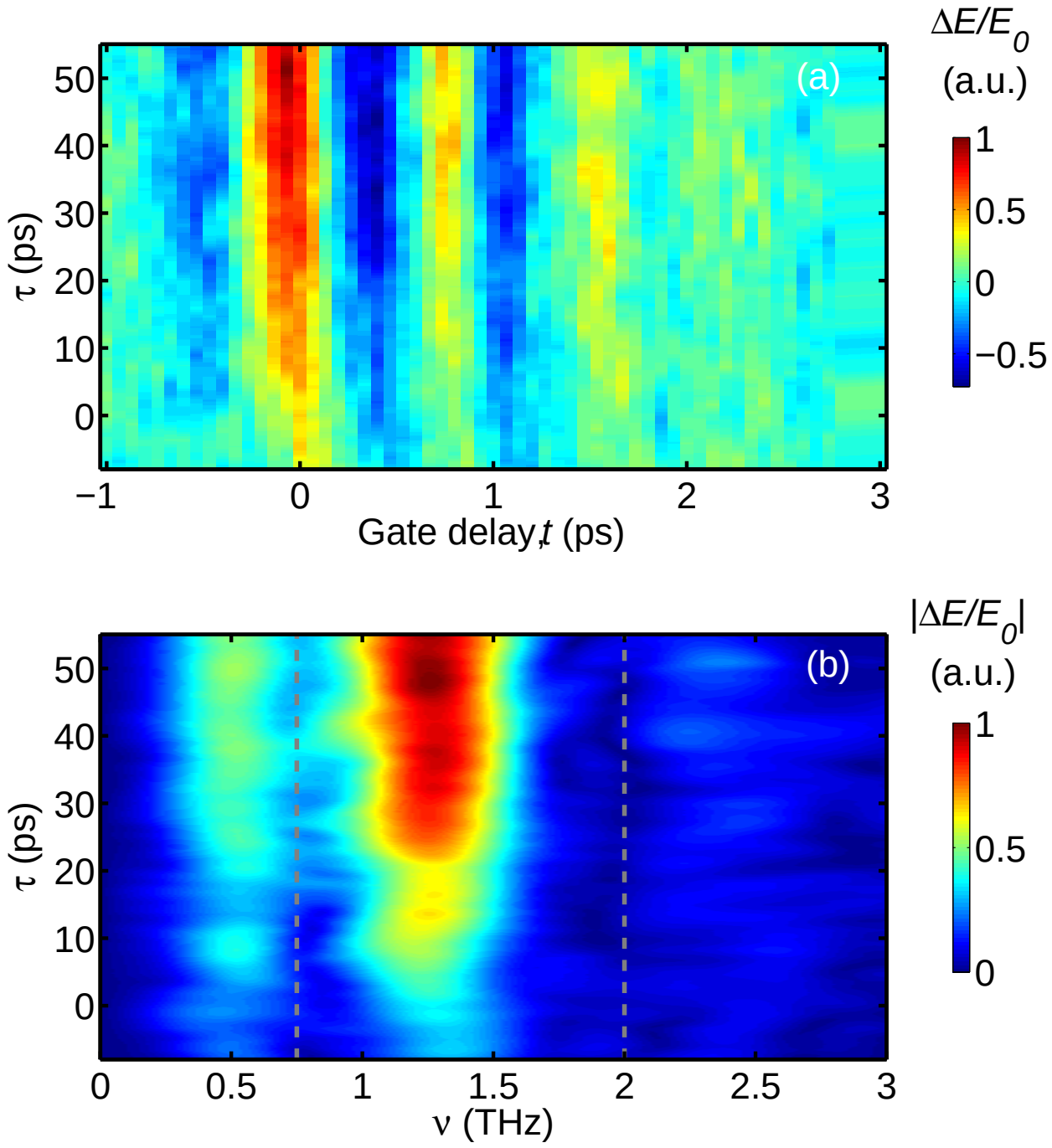

Figure 3 24Oct2016

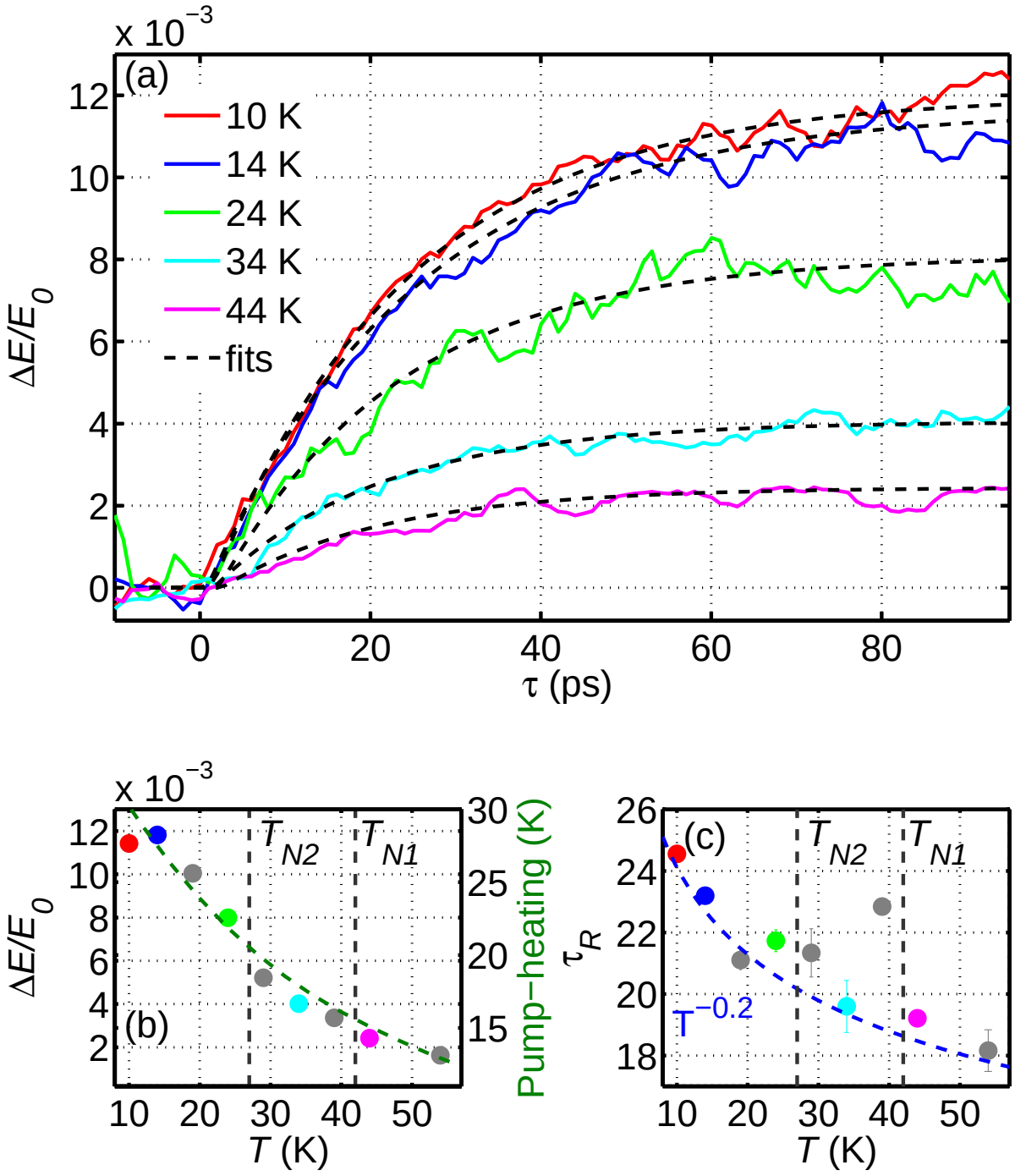

Figure 4 24Oct2016

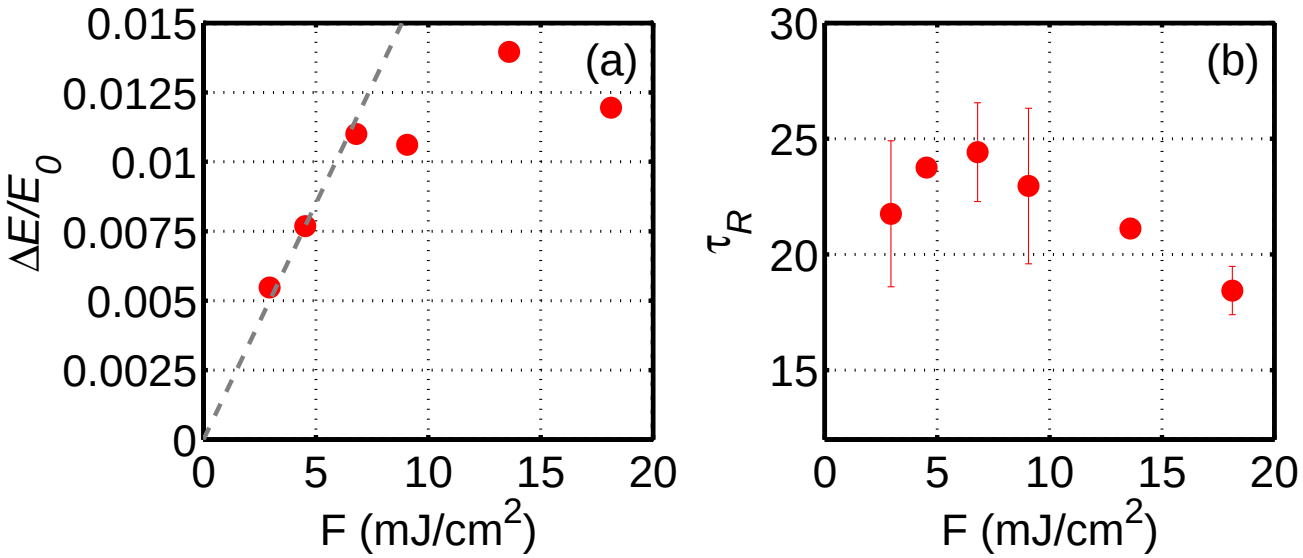

Figure 5 24Oct2016